ELSEVIER

Journal of Alloys and Compounds 317–318 (2001) 485–490

Journal of ALLOYS AND COMPOUNDS

www.elsevier.com/locate/jallcom

Defect structures in FeAl B2 alloys

S. Gialanella[a,*], R.S. Brusa[b], W. Deng[e,1], F. Marino[c], T. Spataru[d], G. Principi[d]

[a]*Dipartmento di Ingegneria dei Materiali, Università di Trento, 38050 Mesiano-Trento, Italy*
[b]*Dipartmento di Fisica and INFM, Università di Trento, 38050 Povo (Trento), Italy*
[c]*Dipartmento di Ingegneria Chimica e Scienza dei Materiali, Politecnico di Torino, C.so Duca degli Abruzzi 24, 10129 Torino, Italy*
[d]*Dipartmento di Ingegneria Mecanica, Settore Materiali and INFM, Università di Padova, Via Marzolo 9, 35131 Padova, Italy*
[e]*Physics Department, Guangxi University, Nanning, China*

Abstract

Two alloys of the Fe–Al system, having compositions in the B2 phase stability range, have been investigated concerning the kinds and concentrations of the lattice defects that can be frozen into the material by water quenching from temperatures as high as 1000°C. The specimens were characterised using positron annihilation methods, Mössbauer spectroscopy and X-ray diffraction. The values of the positron lifetimes indicate that lattice defects in the samples quenched from lower temperatures are different from those found in specimens treated at higher temperatures. The overall picture on the actual type and concentration of such defects, as also obtained from the other analytical techniques, is consistent with the literature data on similar alloys.

Keywords: Ordered structures; Lattice defects; Positron annihilation; Mössbauer spectroscopy; X-Ray diffraction

1. Introduction

Ordered FeAl alloys based on the B2 structure have attracted considerable research interest over the years, not only in connection with technological applications [1], but also for some peculiar microstructural aspects [2]. A feature that is immediately evident upon looking at the relevant phase diagram [3] is the wide composition range over which FeAl is stable, as are other transition metal aluminides, e.g. CoAl, NiAl. Associated with this aspect is the possibility for these materials to host significant concentrations of 'constitutional' point defects, as recently referred to in the most interesting series of papers by Cottrell [4–6]. Actually, this topic has been successively reconsidered and a revision of the principles of point defect formation in B2 phases put forward [7]. In the present context, it is interesting to remark the still standing and widely investigated issue concerning the very high concentrations of thermal point defects which are present in these materials at high temperatures, and the fact that they can be easily retained down to room temperature using not particularly drastic cooling rates. In this respect, both theoretical and experimental studies are copiously present in the literature. We refer the reader to some of the more recent investigations on the subject, using more refined modelling methods and efficient experimental tools, based on Mössbauer spectroscopy [8,9] and positron annihilation experiments, possibly associated with time-differential dilatometry [10–13], to revise older results [14,15].

It is worth remembering that the extensive presence of point defects in intermetallic FeAl-base materials, as in other ordered B2 alloys, has quite sensible effects on yield strength and hardness. This was proven by measuring the hardness of samples cooled down with different cooling rates [16] or by mechanical testing conducted at high temperature [17]. In the latter case, a linear dependence between the alloy yield strength increase and the square root of vacancy concentration was found.

In the present study, two alloys of the Fe–Al system, having compositions in the B2 phase stability range, have been investigated concerning kinds and concentrations of the lattice defects that can be frozen into the material by water quenching from temperatures as high as 1000°C.

The alloy specimens were characterised using hardness testing, positron annihilation methods, Mössbauer spec-

*Corresponding author. Tel.: +39-0461-882-420; fax: +39-0461-881-977.

E-mail address: stefano.gialanella@ing.unitn.it (S. Gialanella).

[1]Present address: Dipartmento di Fisica and INFM, Università di Trento, 38050 Povo (Trento), Italy.

0925-8388/01/$ – see front matter
PII: S0925-8388(00)01375-X

troscopy and X-ray diffraction. The results provide clear indications on the dominant defects present in the alloy materials with different compositions and tempers.

2. Experimental

Two alloy ingots, with nominal compositions Fe–40Al and Fe–48Al (at. %), were prepared by induction co-melting under an argon atmosphere pure element pellets. The ingots were homogenised for 96 h at 1000°C and then furnace cooled. Alloy specimens, having dimensions 10×10×2 mm^3, were spark eroded before the quenching treatments. Pairs of samples of each composition were put inside a tubular furnace under flowing argon at the set temperature. A thermocouple was kept in contact with the specimens to record the exact time when the selected temperature was achieved. The samples were left in the furnace for 5 min. Three temperatures have been considered: 500, 800 and 1000°C. In all cases the pre-existing oxide layer, present on the alloy samples after the cutting operations, and the inert gas flow prevented any further oxidation occurring. The alloy specimens were then metallographically polished on one base face before further characterisation. Microhardness tests were conducted on the polished face of the specimens with a Vickers indenter loaded with 50 g.

X-Ray diffraction analyses were carried out to measure the lattice parameter using a wide angle diffractometer with CuKα radiation monochromated on the diffracted beam.

Positron lifetime measurements were carried out at room temperature by using a fast–fast coincidence system (Hamamatsu R2083Q photomultipliers with BaF_2 scintillators and fast discriminators) with a time resolution of 180 ps full width at half maximum (FWHM) [18]. After source correction (lifetime τ_s=382 ps; intensity I_s=6%) and background subtraction, all the spectra were analysed by using the Positronfit Extended program. Three lifetime components have been identified in each spectrum: a short lifetime τ_1 (varying in the 178–197 ps range), an intermediate lifetime τ_2 (ranging between 300 and 800 ps) with a small intensity (around 3%) and a long lifetime τ_3 (around 1500 ps). The long-life component τ_3 in each spectrum, with a very small intensity (0.2%), is due to positron annihilation at the surface of the sample or in the source, and will be disregarded in our discussion.

Doppler broadening spectra were measured using a two-detector coincidence system. The main detector was a high-purity Ge (HPGe) detector (16% efficiency) with a resolution of 1.3 keV at 511 keV with 2 s shaping time in the HPGe spectroscopy amplifier. A pileup rejection signal was used to gate the multichannel analyser (MCA). The auxiliary detector supplying the coincidence signal was a NaI(Tl) scintillator. The NaI(Tl) detector was placed in collinear geometry with the Ge detector in order to detect the two 511 keV gamma rays from the e^+–e^- annihilation pair. The annihilation event was accepted in the MCA if both annihilation photons were detected in coincidence in the HPGe and NaI(Tl) detectors. With this set-up, we get a peak to background ratio of about 1×10^4 on the high energy side of the peak (at 530 keV). In these measurements the momentum component p_z of the positron electron annihilation pair in the direction of the detector is measured. The momentum p_z is related to the Doppler shift ΔE by the formula $p_z=2\Delta E/c$, where c is the light velocity. The magnitude of the positron annihilation with low momentum can be investigated by means of the usual S parameter. The S parameter is calculated as the ratio of the counts in the central area of the peak [$0\leq(E_\gamma-511$ keV$)\leq0.776$ keV] and the total area of the peak [$0\leq(E_\gamma-511$ keV$)\leq9.31$ keV]. The S parameter reflects the fraction of positrons annihilating with electrons of low momentum. An increase of the S parameter is an indication of positron trapping in open volume defects.

Mössbauer spectra of the samples were measured at room temperature with a standard constant acceleration spectrometer, using a ^{57}Co:Rh source and an Ar10%–CH_4 flowing gas proportional detector to reveal X-rays emitted after resonant absorption of gamma rays. This allowed one to obtain structural information on sample surface layers of the same approximate thickness explored by X-ray diffraction. A specific current minimisation routine was used to fit the experimental profiles, according to the model proposed in Ref. [19], in which a careful evaluation of Mössbauer experimental data, taken also at low temperature and with external magnetic field on samples having about the equiatomic composition, was based on calculations of interatomic distances and hyperfine parameters. In this model four spectral components were recognised corresponding to four inequivalent sites for iron atoms: (1) ordered B2 sites; (2) neighbours of a iron vacancy; (3) atoms in wrong position, i.e. antisite atoms (AS), (4) corner atoms of AS atoms.

3. Results

The quenching treatments described above were conducted on samples preliminarily annealed for 96 h at 1000°C and then furnace cooled. This treatment was meant to homogenise possible composition fluctuations. The slow cooling rate should have reduced any trapping phenomena of thermal defects which were present at the annealing temperature. In this way, reference samples were produced to better evaluate the changes brought about by the water-quenching treatments. In Fig. 1 the hardness curves vs. S parameter for the two compositions, Fe–40Al and Fe–48Al, are shown. The corresponding quenching temperatures are indicated in the graphs. With some differences in the relative values and trends, both alloys display an increase in hardness as the quenching temperatures are

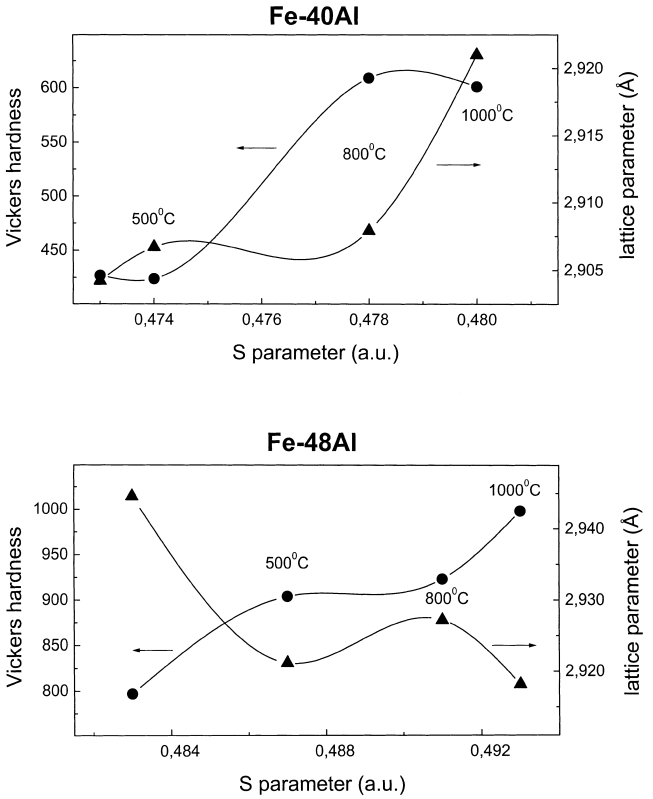

Fig. 1. Hardness and lattice parameter curves vs. *S* parameter for the two alloys Fe–40Al and Fe–48Al (at. %). The *S* parameter was evaluated for alloy samples quenched from the temperatures indicated in the graphs. The starting points correspond to fully annealed and homogenised specimens.

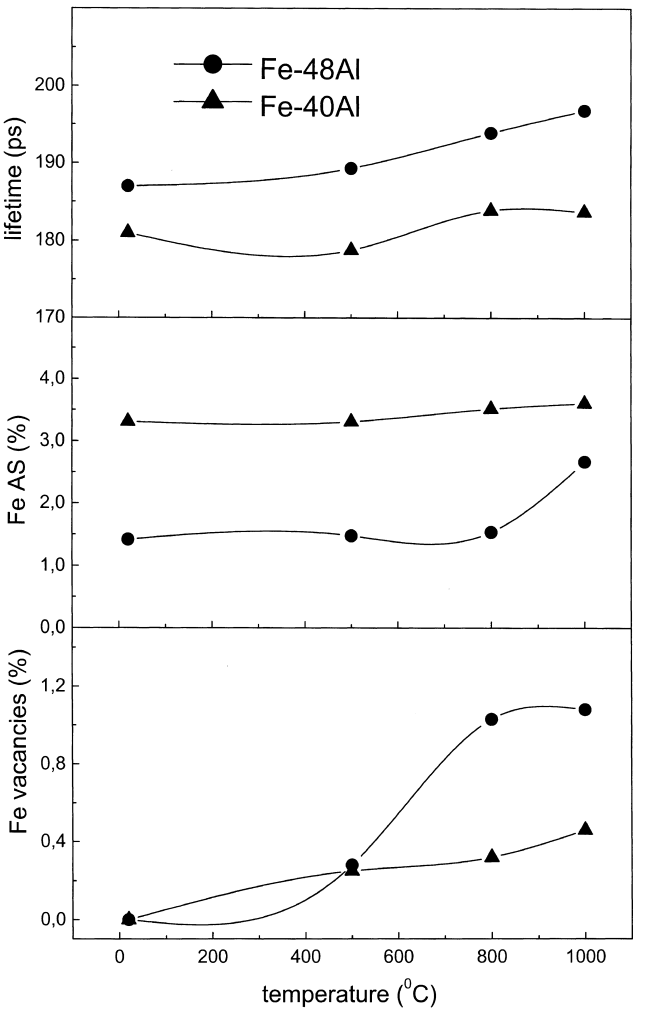

Fig. 2. Lifetime (τ_1), concentration of Fe antisites and vacancies vs. quenching temperature for the two alloys Fe–40Al and Fe–48Al (at. %).

increased. This increase in hardness can be straightforwardly related to the increase of thermal vacancy concentration, in agreement with the observed increasing values of the *S* parameter.

X-Ray diffraction analyses indicated the two reference alloys to have a B2 ordered structure, which was the only phase detected even after the quenching treatments that, on the other hand, had some effects on the lattice parameter. This is illustrated in Fig. 1 where, for an easier comparison with other microstructural parameters, the lattice parameter too is plotted as a function of the *S* parameter. In the Fe–40Al alloy a lattice expansion is observed, with the major increase in the sample quenched from 1000°C. A completely different behaviour is displayed by the Fe–48Al alloy, for which the quenching treatments induce a lattice contraction, quite significant already at the lower quenching temperature (500°C).

Positron lifetime values provide further insight on the kind of defects which actually formed in the material. Fig. 2 shows the evolution of τ_1 lifetimes for the Fe–40Al and Fe–48Al alloys as a function of the quenching temperature. In the Fe–40Al material the lifetime value for the sample quenched from 500°C is the same as the one obtained with the reference sample (fully annealed and slow cooled). A slight increase can be noticed in the samples quenched from 800 and 1000°C. Larger lifetimes were measured for the Fe–48Al alloy. In this case, a continuous increase was noticed in the samples quenched from higher temperatures, which displayed larger values than the reference material.

Mössbauer spectroscopy data indicated how the site occupation was modified in the two alloys by the quenching treatments. All patterns in Fig. 3a and b display a broad paramagnetic single peak which can be actually resolved into several components, according to the model of Ref. [19] (see Section 2). Together with the experimental points the fitting curves corresponding to the most likely and important contributions are displayed. The computed hyperfine parameters are reported in Table 1 explicitly for iron atoms: (1) in ordered B2 sites, represented by a singlet; (2) as neighbours of an iron vacancy, represented by a doublet; (3) in the AS position, represented by a singlet; (4) as corner atoms of ASs, repre-

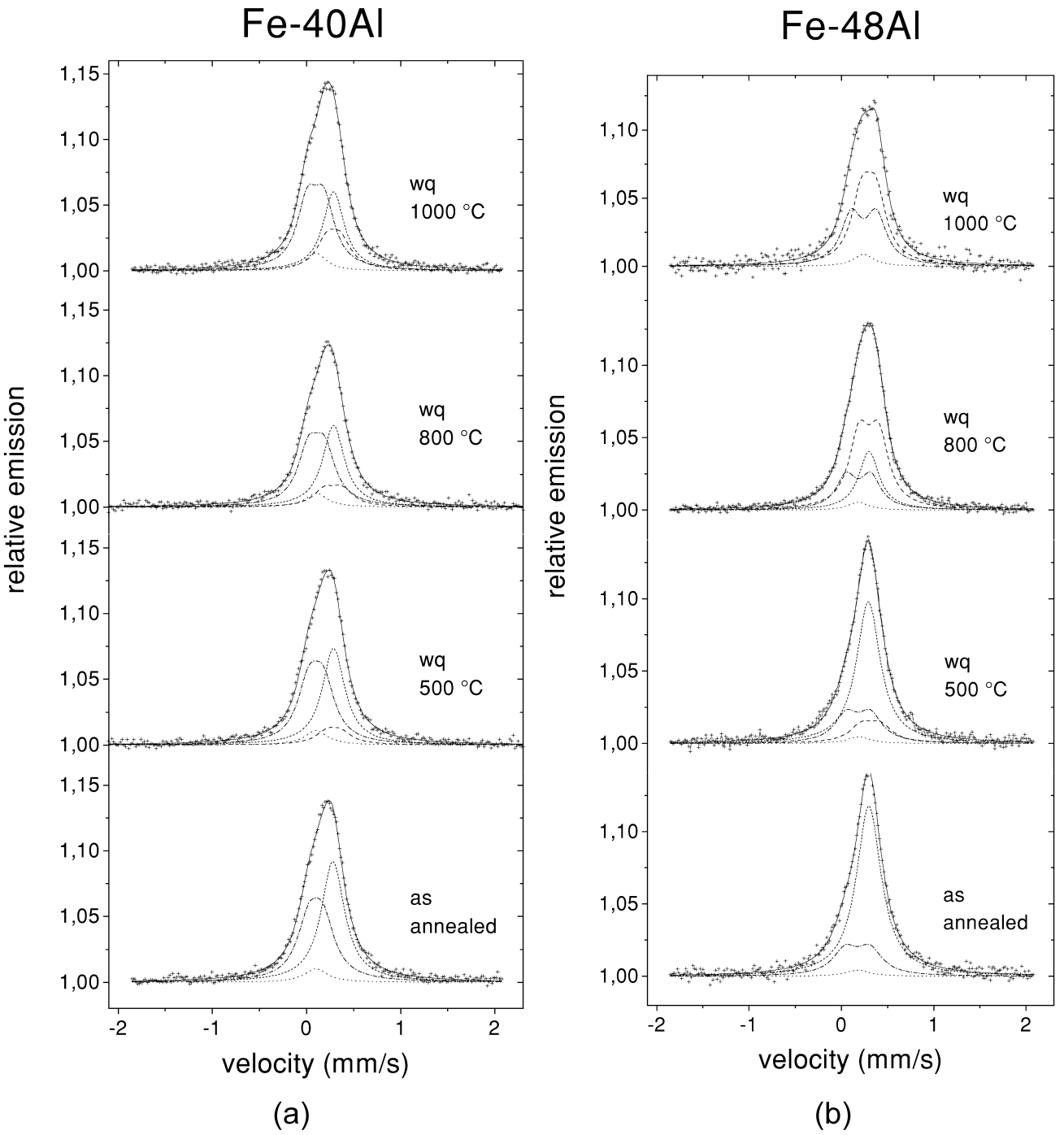

Fig. 3. Conversion X-ray Mössbauer spectra of: (a) Fe–40Al and (b) Fe–48Al (at. %) alloy samples after the treatments indicated in the graphs. Graph legend: data points (crosses); best fit (solid line); Fe antisite atoms (dots); neighbours of Fe antisites (dash–dot); ordered B2 (short–dash); neighbour of Fe vacancy (dash).

sented by an unresolved sextet and described by a doublet. Some constraints have been used: (i) equality of all linewidths, on the assumption that all iron sites are equally disturbed in the same sample; (ii) area ratio of 8 between corner atoms of AS and AS; (iii) equality of δ values for corner atoms of AS and AS; (iv) fixed values for some parameters, underlined in Table 1, in order to obtain consistency with related parameters and literature data and models. The reported values of iron AS and vacancy concentrations are also visualised in Fig. 2.

Table 1
Computed Mössbauer parameters in Fe–48Al and Fe–40Al samples: δ, isomer shift; Δ, quadrupole splitting (see text)

Sample	Quenching temperature (°C)	Ordered B2, δ (mm/s)	Vacancies (at. %)	Neighbours of Fe vacancy		Corner atoms around Fe AS			Fe AS atoms (at. %)
				δ (mm/s)	Δ (mm/s)	at. %	δ (mm/s)	Δ (mm/s)	
$Fe_{52}Al_{48}$	As annealed	0.30	–	–	–	11.38	0.18	0.27	1.42
	500	0.29	0.28	0.32	0.20	11.85	0.18	0.27	1.48
	800	0.29	1.03	0.30	0.21	12.30	0.18	0.27	1.54
	1000	–	1.08	0.30	0.15	21.35	0.24	0.27	2.67
$Fe_{60}Al_{40}$	As annealed	0.28	–	–	–	26.43	0.10	0.15	3.31
	500	0.29	0.25	0.29	0.18	26.43	0.10	0.16	3.31
	800	0.29	0.32	0.29	0.18	26.44	0.11	0.17	3.52
	1000	0.29	0.46	0.29	0.15	26.72	0.10	0.16	3.61

4. General discussion

The aim of the research was to evaluate and characterise the point defect structures which can be trapped in FeAl alloys based on the B2 structure through water quenching from high temperatures. An evident effect of the quenching treatments, which were actually carried out on alloy samples with Fe–40Al and Fe–48Al compositions, was a general increase in the hardness of the two alloys (Fig. 1). Similar results have been already obtained with this kind of B2 alloy [16,17] as a consequence of an enhanced resistance to dislocation movement due to thermal point defects, particularly vacancies. Indeed, the S parameter presented in the hardness plots is an increasing function of thermal vacancy concentration. From the analysis of other available data it is possible to better characterise the structure of the defects these vacancies are taking part into. Lifetime values (Fig. 2) are in excellent agreement with those found for FeAl alloys with compositions similar to ours [11,12]. In the Fe–40Al the 180 ps lifetime can be associated with single vacancies possibly organised as triple defects, i.e. two vacancies plus an antisite. Although more complex, a triple defect has an electron density and, thereby, positron sensitive volume comparable to those of a single vacancy. This is so because the two vacancies are not located in next neighbours sites. At higher quenching temperature, lifetimes indicate the presence of larger defects. This cannot be ascribed to the temperature dependence of the vacancy formation volume, as would be the case for Fe–Al alloys with Al concentrations up to 25 at. % [20,21]. The lifetime increase cannot be justified in terms of formation only of larger defects, e.g. divacancy, as it will be seen to occur in the Fe–48Al alloy (Fig. 2). It is possible to conclude that the slight lifetime increase when quenching from 800 and 1000°C the Fe–40Al material is still mainly an effect of triple defects with some minor contribution from divacancies.

Accordingly with this interpretation, Mössbauer results indicate only little changes in the vacancy concentration as the quenching temperature is increased from 800 to 1000°C (Fig. 2). Antisite defect concentration (Fig. 2), in excess with respect to the constitutional value, has the same value in the annealed and 500°C quenched Fe–48Al samples; it becomes higher in the samples quenched from 800 and 1000°C. For the Fe–40Al samples a prevailing presence of antisite defects and a lattice expansion were observed (Fig. 1). Incidentally, this datum would agree with similar results obtained with rapidly solidified Fe–Al alloys [22] and upon disordering by ball-milling a Fe–40Al powder [23].

A lattice contraction with quenching was observed in the Fe–48Al alloy, indicating the presence of another kind of predominant defect. Going back to the lifetimes for this alloy (Fig. 2), the experimental values increase smoothly even from the low quenching temperature. From the evolution of the curve we can infer the presence at low temperatures of single vacancies and triple defects. Divacancies start to be present, to minor extent, in the 500°C quenched samples, but become the majority defects at higher temperatures [11]. Mössbauer results confirm particularly high vacancy concentrations in the 800 and 1000°C quenched samples (Fig. 2). Fe antisites remain comparatively lower than in the other material, also for compositional reasons, although their still significant and well detectable presence confirms vacancies to occur mainly in vacant Fe sites. High concentrations of single and double vacancies not only justify the cited reduction in the lattice parameter but also high hardness increase with quenching temperature (Fig. 1).

To complete the picture of the positron annihilation data, it is worth mentioning that also another lifetime (τ_2) with a small intensity (3%) was found from the spectral analysis. τ_2 ranged from 290 ps (annealed reference sample) to 450 ps for the Fe–40Al alloy and from 290 to 850 ps for the Fe–48Al alloy. These lifetimes can be tentatively ascribed to grain boundary microcracks, re-

sulting from the thermomechanical stresses associated with the quenching procedures. As a matter of fact, typical lifetimes of positron annihilation at metallic surfaces are 450 ps approximately [24]. This interpretation, which is being further investigated, was suggested also by the extensive fracturing occasionally observed in the alloy specimens, particularly the Fe–48Al, when quenched from 1000°C.

5. Conclusions

The present investigation has dealt with defect structures which can be trapped by water quenching into two FeAl B2 alloys: Fe–40Al and Fe–48Al (at. %). Alloy compositions and quenching temperatures will affect strongly the actual dominant defect. The values of the positron lifetimes and Mössbauer data indicate in the Fe–40Al alloy single vacancy and triple defects to be the main defects for all temperatures. Defects trapped into the Fe–48Al alloy when quenching it down from low temperature (500°C) are different from those found in specimens treated at higher temperatures. Indeed, at low quenching temperature the Al-rich alloy displays the same situation as in the Fe–40Al alloy, with single vacancies and triple defects. At higher quenching temperatures divacancies become the main defects. Hardness was found to increase in any case with quenching temperature. As to lattice parameter, an expansion was observed in Fe–40Al alloy when triple defects predominate. In the Fe–48Al alloy high vacancy concentrations resulted in a lattice shrinkage.

The presence of other larger defects was detected. They can be tentatively associated with microcracks which formed, mainly along the alloy grain boundaries, as a consequence of the thermomechanical stresses of the quenching procedures. In this respect, the proposed approach may be profitably adopted for the characterisation of grain boundary regions, of great importance in determining the macroscopic properties of these materials.

Acknowledgements

Partial financial support of the present work has been obtained from the Italian Ministero della Ricerca Scientifica e Tecnologica in the framework of a National Research Project entitled ‘Leghe e Composti Intermetallici. Stabilità Termodinamica, Proprietà Fisiche e Reattività’.

References

[1] C.G. McKamey, in: Physical Metallurgy and Processing of Intermetallic Compounds, Chapman Hall, 1996, p. 351.
[2] J.H. Westbrook, R.L. Fleischer, Intermetallic Compounds – Principles and Practice, Wiley, New York, 1994.
[3] T.B. Massalski (Ed.), Binary Alloy Phase Diagrams, ASM International, Materials Park, OH, 1990.
[4] A.H. Cottrell, Intermetallics 3 (1995) 341.
[5] A.H. Cottrell, Intermetallics 4 (1996) 1.
[6] A.H. Cottrell, Intermetallics 5 (1997) 467.
[7] X. Ren, K. Otsuka, M. Kogaci, Scripta Mater. 41 (1999) 907.
[8] G. Vogl, B. Sepiol, Acta Metall. Mater. 42 (1994) 3175.
[9] R. Feldwisch, B. Sepiol, G. Vogl, Acta Metall. Mater. 43 (1995) 2033.
[10] R. Würschum, C. Grupp, H.-E. Schaefer, Phys. Rev. Lett. 75 (1995) 97.
[11] J. Wolff, M. Franz, A. Broska, B. Köhler, T. Hehenkamp, Mater. Sci. Eng. A239–240 (1997) 213.
[12] B. Köhler, J. Wolff, M. Franz, A. Broska, T. Hehenkamp, Intermetallics 7 (1999) 269.
[13] H.-E. Schaefer, K. Frenner, R. Würschum, Intermetallics 7 (1999) 277.
[14] J.P. Riviere, J. Grilhe, Acta Metall. 20 (1972) 1275.
[15] D. Paris, P. Lesbats, J. Nucl. Mater. 69–70 (1978) 628.
[16] P. Nagpal, I. Baker, Metall. Trans. A22 (1990) 2281.
[17] I. Baker, E.P. George, Phil. Mag. A77 (1998) 737.
[18] J. De Vries, A. Zecca, R.S. Brusa, R.G. Grisenti, S. Ossi, Nucl. Instrum. Methods A275 (1989) 194.
[19] J. Bogner, W. Steiner, M. Reissner, P. Mohn, P. Blaha, K. Schwartz, R. Krechler, H. Ipser, B. Sepiol, Phys. Rev. B58 (1998) 14922.
[20] J. Wolff, M. Franz, T. Hehenkamp, J. Radioanal. Nucl. Chem. 210 (1996) 591.
[21] J. Wolff, M. Franz, T. Hehenkamp, Microchem. Acta 125 (1997) 263.
[22] S. Gialanella, F. Marino, in: Kinetics of Ordering Transformations in Metals, TMS, Warrendale, PA, 1992, p. 359.
[23] S. Gialanella, Intermetallics 3 (1995) 73.
[24] K.G. Lynn, W.E. Frieze, P.J. Schultz, Phys. Rev. Lett. 52 (1984) 1137.